Building a Photocatalyst Library of MR-TADF Compounds with Tuneable Excited-State Redox Potentials

Lea Hämmerling[1] and Eli Zysman-Colman[1]*

[1]Organic Semiconductor Centre, EaStCHEM School of Chemistry, University of St Andrews;
St Andrews, KY16 9ST, United Kingdom.

*Corresponding author. Email: eli.zysman-colman@st-andrews.ac.uk

Abstract

Epitomised by **4CzIPN**, donor-acceptor (D-A) thermally activated delayed fluorescence (TADF) compounds based on the carbazoyl dicyanobenzene have now become widely used as they are sustainable photocatalyst alternatives to organometallic complexes owing to their similar optoelectronic properties to many of the iridium-based photocatalysts. Multi-resonant TADF (MR-TADF) compounds offer distinct advantages over D-A TADF compounds as they have more intense low-energy absorption bands, offering faster reaction kinetics, and are less sensitive to the polarity of the environment, mitigating undesired energy loss that typically accompanies the CT excited states of the photocatalysts. Here we report the assessment of strongly photoreducing boron- and nitrogen-doped MR-TADF compounds **DABNA-1**, ***t*DABNA**, **CzBN** and **DtBuCzB** across a range of benchmark photochemical reactions. The structural differences between each member of this library of photocatalysts enables modulation of their ground- and excited-state redox potentials. These photocatalysts performed competitively compared to the literature-known **4CzIPN**, **Ph-PTZ** and ***fac*-Ir(ppy)$_3$**.

Introduction

Photocatalysis has cemented itself as an important tool for synthetic organic chemists, allowing for thermally inaccessible transformations to be conducted at room temperature utilising visible light energy as the driving force.[1-3] During a photocatalytic reaction, the photocatalyst (PC) is excited into an excited state (PC*) by absorbing incident visible light. After rapid internal conversion processes the PC* can subsequently interact with substrates (S) in several different ways. If the PC* transfers its energy to S, the activation mode is termed photoinduced energy transfer (PEnT), and can occur via either a Dexter or a Förster energy transfer mechanism.[4] If the interaction involves single-electron transfer, the mechanism is termed photoinduced electron transfer (PET), occurring via oxidative quenching (where the PC* is initially oxidised to PC$^{+\bullet}$ and S is reduced to S$^{-\bullet}$) or reductive quenching (where the PC* is reduced to PC$^{-\bullet}$ and

S is oxidised to $S^{+\bullet}$) catalytic cycles. Collectively, PET photocatalalysis is commonly referred to as photoredox catalysis.

In homogenous photocatalysis, broadly, PCs can be divided into two main families: transition metal complexes and organic photocatalysts. The initial explosion of interest in photocatalytic reactions over the past 15 years or so has been accompanied by the frequent use of organometallic Ru(II) and Ir(III) complexes as photocatalysts (Figure **S2**), which interact with substrates exclusively from their triplet excited state. Despite their ability to photocatalyze a wide range of reactions, the platinoid metals are scarce and costly and the toxicity profile is suboptimal, particularly if late-stage photocatalysis is to be used in pharmaceutical synthesis.[5-7] The most prominent organic PCs are either natural organic dyes, like Eosin Y,[8,9] Rose Bengal,[10,11] fluorescein,[5,12,13] and acridinium salts,[14,15] or donor-acceptor (D-A) thermally activated delayed fluorescent (TADF) emitters originally designed for use in organic light-emitting diodes.[3,16]

Unlike fluorescent dyes, the singlet (S_1) and triplet (T_1) excited states of TADF compounds are both populated, facilitated by a small energy gap (ΔE_{ST}) between the two that permits exciton cycling by a combination of intersystem crossing (ISC) and reverse intersystem crossing (RISC). The small ΔE_{ST} results from the small exchange integral between the highest occupied molecular orbital (HOMO) and lowest unoccupied molecular orbital (LUMO). In donor-acceptor TADF emitters, this separation is most commonly achieved when the donor and acceptor adopt a strongly twisted conformation such that electronic communication between the two is very weak. Luo *et al.*[17] first demonstrated that prototypical TADF carbazolyl dicyanobenzenes (CDCBs) like **4CzIPN** (Figure ***2*f**, Figure **S1a**) can be highly efficient visible-light PCs. Due to its remarkably similar photophysical properties to the widely used photocatalyst **[Ir(dF(CF$_3$)-ppy)$_2$(dtbbpy)]PF$_6$**, **4CzIPN** has been repeatedly shown to be a highly versatile and competitive photocatalyst across a broad range of transformations.[3] Modulating the structure of **4CzIPN** and its derivatives results in the facile tuning of their ground and excited state redox potentials, making this class of PCs much more versatile than the naturally occurring organic dyes historically used for photocatalysis.[17,18] Beyond **4CzIPN** and structurally related PCs, a small number of other D-A TADF compounds have been explored as PCs. Recently, we reported that **pDTCz-DPmS** (Figure **S1b**) was a versatile PC across a range of photocatalytic reactions.[19] Bouzrati-Zerelli *et al.* used a similar D-A PC containing electron-deficient diphenyl sulfone to initiate a free radical polymerisation of methacrylates.[20] Hojo *et al.* showed that a group of imidazophenothiazine (**IPTZ**)-based TADF emitters (Figure **S1c**) can serve as efficient photocatalysts in five different PEnT reactions.[21]

This work built upon related imidazoacridine-based TADF compounds that were demonstrated to photocatalyse [2+2] cycloadditions in a PEnT mechanism.[22]

a) Previous examples of MR-TADF photocatalysts

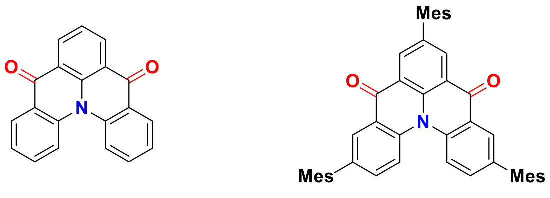

DiKTa **Mes$_3$DiKTa**

Chem. Eur. J., **2023**, *29*, e202202998

b) This work: Boron-Nitrogen doped MR-TADF photocatalysts

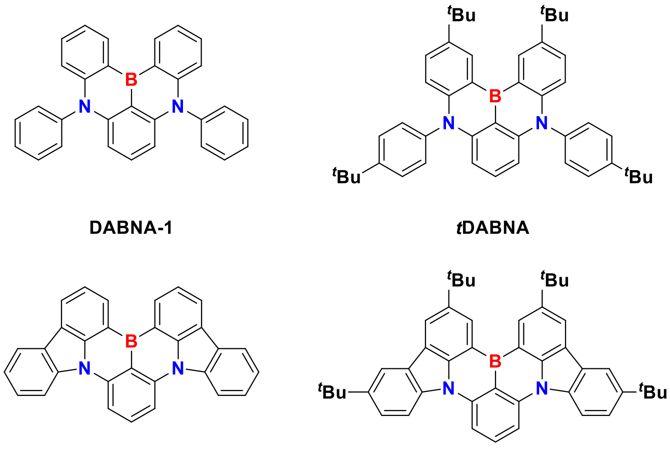

DABNA-1 ***t*DABNA**

CzBN **DtBuCzB**

Figure **1**. a) Structures of previous examples of multi-resonant thermally activated delayed fluorescence (MR-TADF) photocatalysts (PC) **DiKTa** and **Mes$_3$DiKTa**.b) This work: Boron-Nitrogen doped MR-TADF photocatalysts.

We demonstrated that the multi-resonant TADF (MR-TADF) emitters **DiKTa** (E_{red}* = 1.49 V and E_{ox}* = -1.16 V in MeCN[23]) and **Mes$_3$-DiKTa** (E_{red}* = 1.35 V and E_{ox}* = -1.04 V in MeCN[17]) are attractive compounds as PCs (

Figure **1a**), matching or even outperforming D-A TADF and organometallic PCs across a mechanistically broad range of reactions**Error! Reference source not found.**.[23] MR-TADF emitters are typically n- and p-doped nanographene compounds that have short-range charge transfer (SRCT) excited states that lead to relatively small ΔE_{ST}.[24] Importantly, the SRCT stare is less strongly influenced by the polarity of the solvent than long-range CT (LRCT) states of D-A TADF compounds, meaning that less energy is lost in these compounds in polar solvents.[24] As well, due to their rigid structure, there is less geometric reorganization in the excited state, leading to bright, narrowband emission and intense low-energy absorption bands The high molar absorptivity in the visible region of these bands is beneficial in photocatalysis as it means that the concentration of PC* is higher and the rate of the reaction is generally faster.

Strongly photoreducing literature organic PCs include **Ph-PTZ** (**PTH**), **AZ1**, and **AZ2**Error! Reference source not found., possessing excited-state oxidation potentials, E_{ox}* of -2.10,[25] -2.34,[26] and -2.36 V,[26] respectively (Figure ***2*****a-c**). Unfortunately, the low-energy absorption bands of each of these PCs have low molar absorptivity (**Ph-PTZ**: λ_{abs} = 300 nm in MeCN, ε not quantified,[27] **AZ1** and **AZ2**: λ_{abs} = 373 nm, $\varepsilon = 5.2 \times 10^3$ $M^{-1}cm^{-1}$ and λ_{abs} = 370 nm, $\varepsilon = 4.9 \times 10^3$ $M^{-1}cm^{-1}$ in DMF).[26] Therefore, a strongly photoreducing PC possessing an intense low-energy absorption band in the visible region would be highly desirable. Despite the significant promise of these MR-TADF molecules, **DiKTa** and **Mes$_3$DiKTa** are only moderately photoreducing (E_{ox}* = -1.16 and -1.05 V, respectively) yet are strong photooxidizing agents (E_{red}* = 1.49 and 1.31 V for **DiKTa** and **Mes$_3$DiKTA**, respectively) (Figure ***2*****d**, **e**)Figure ***3***. These two photocatalysts should therefore have behave similarly to **4CzIPN** (E_{ox}* = -1.04 and E_{red}* = 1.35 V[17]) and thus would not be appropriate to use in reactions that require more highly photoreducing catalysts. We thus targeted identifying MR-TADF compounds that would be more stronger photoreducing and still leverage the distinct advantages of the photophysical properties endemic to this class of compounds.

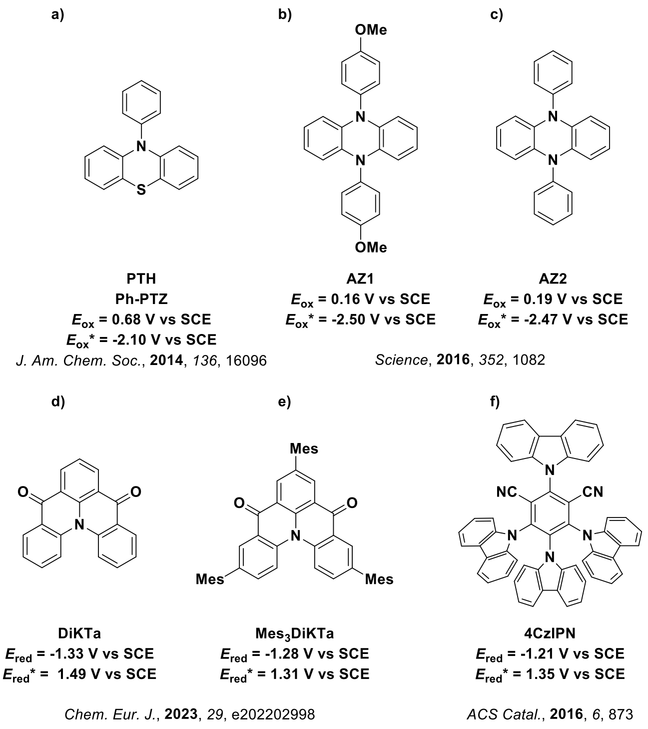

J. Am. Chem. Soc., **2014**, *136*, 16096

Science, **2016**, *352*, 1082

Chem. Eur. J., **2023**, *29*, e202202998

ACS Catal., **2016**, *6*, 873

Figure **2**. Chemical structures of literature known strongly photoreducing photocatalysts (a) **Ph-PTZ**, (b) **AZ1** and (c) **AZ2** as well as the strong photooxidising photocatalysts (d) **DiKTa**, (e) **Mes$_3$DiKTa**, and (f) **4CzIPN**. Mes = mesityl

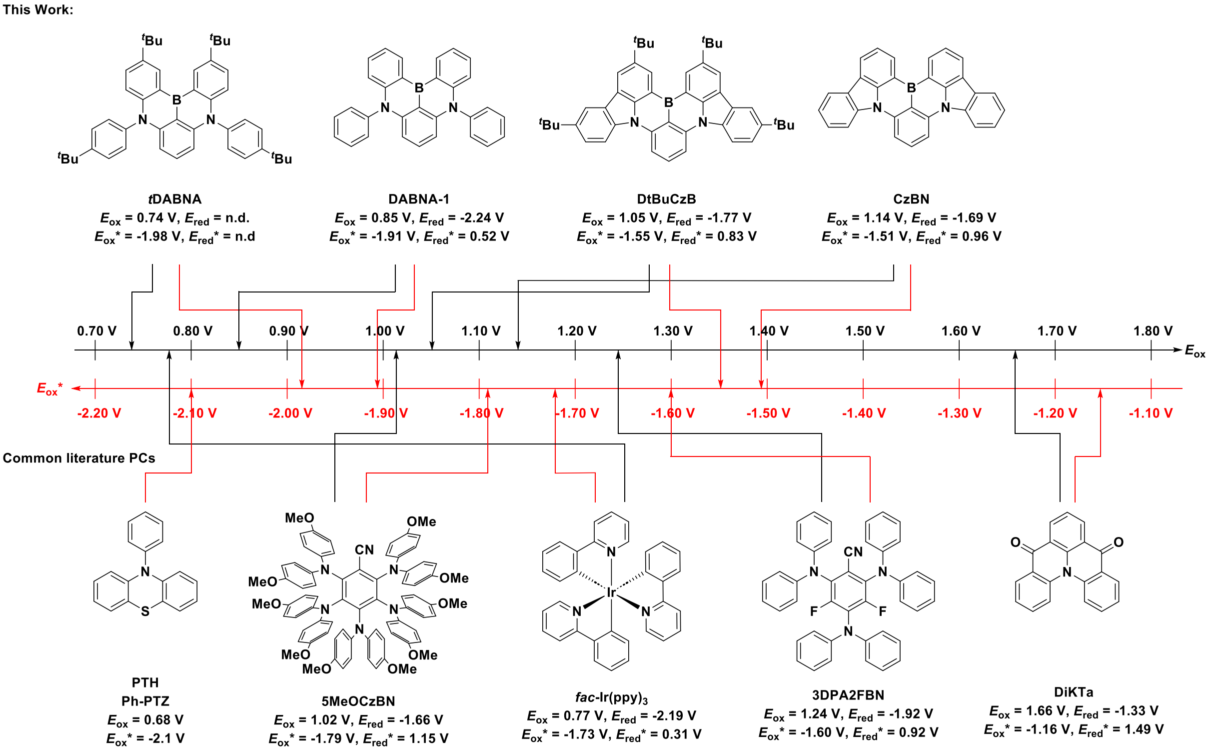

Here, we investigated four boron/nitrogen MR-TADF emitters as PCs. These include: **DABNA-1**, first reported by Hatakeyama *et al.* (**Figure *3***),[28] which has an intense absorption band in DCM at λ_{abs} of 437 nm ($\varepsilon = 24.6 \times 10^3$ M^{-1} cm^{-1});[28] a *tert*-butyl-substituted derivative ***t*DABNA** that has a slightly red-shifted, intense absorption band at λ_{abs} of 445 nm[29] though the authors did not report its molar absorptivity; a carbazole analogue to **DABNA-1**, **CzBN** that has a red-shifted absorption band at λ_{abs} of 457 nm in toluene;[30] and a *tert*-butyl-substituted analogue, **DtBuCzB**, that possesses the most red-shifted absorption band of the four compounds at λ_{abs} of 467 nm in toluene.[31] For the latter two compounds, no molar absorptivity data were reported. The four photocatalysts are each strongly photoreducing, ranging from **CzBN** (E_{ox}* = -1.51 eV) to ***t*DABNA** (E_{ox}* = -1.98 eV) (Figure **3**). These have comparable photoreducing strength to recognized strongly photoreducing literature photocatalysts ***fac*-Ir(ppy)₃** (E_{ox}* = -1.73 V) and **Ph-PTZ** (E_{ox}* = -2.10 V) (Figure **3**).

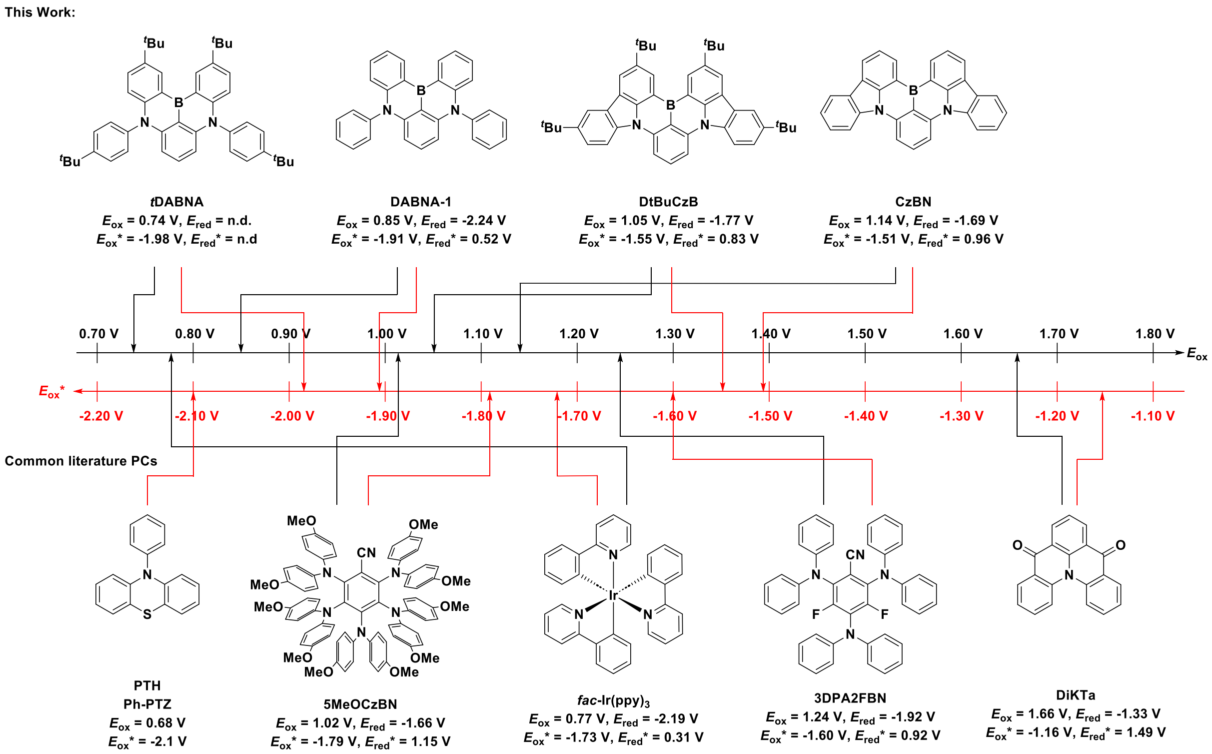

Figure **3**. Structures and redox potentials of the MR-TADF emitters investigated as photocatalysts in this work and a comparison to literature known photocatalysts (redox potentials of **Ph-PTZ** taken from ref. [32] in MeCN, **3DPA2FBN** and **5MeOCzBN** taken from ref. [18] in MeCN and ***fac*-Ir(ppy)₃** from ref. [33,34] in MeCN).

Results and Discussion

Synthesis and photophysical investigations

DABNA-1, ***t*DABNA**, **CzBN** and **DtBuCzB** were synthesised using a two-step protocol that was adapted from the literature (Figure **S4**). The overall unoptimized yields were 12, 19, 37 and 32% for **DABNA-1**, ***t*DABNA**, **CzBN** and **DtBuCzB**, respectively, with the bromination being the yield-limiting step in the synthesis. The photophysical and electrochemical properties of **DABNA-1**, **tDABNA**, **CzBN** and **DtBuCzB** were investigated in toluene (PhMe), THF, DCM, MeCN and DMF, commonly used solvents for photocatalysis reactions, and their properties cross-compared to those of the archetypal TADF PC **4CzIPN**. Cyclic voltammetry (CV) and different pulse voltammetry (DPV) scans of **DABNA-1** are shown in Figure **S25a**. In MeCN and DMF, the reduction was found to be irreversible at E_{red} of -2.24 and -2.14 V vs SCE, respectively, values that are comparable to the literature PC ***fac*-Ir(ppy)$_3$** (E_{red} of -2.19 V vs SCE in MeCN[33]); no reduction was observed in THF or DCM as the electron affinity lies beyond the solvent window. The oxidation of **DABNA-1** is irreversible in THF, MeCN and DMF but reversible in DCM. The E_{ox} values are broadly similar in DMF, MeCN and DCM at E_{ox} of 0.86 0.80 and 0.85 V vs SCE, respectively; however, this changes significantly in THF (E_{ox} of 1.01 V), possibly due to the formation of a THF adduct upon oxidation. The oxidation potentials are more positively shifted than of ***fac*-Ir(ppy)$_3$** (E_{ox} of 0.77 V vs SCE in MeCN[33]). Due to the reduced solubility of ***t*DABNA**, the CV and DPV could only be recorded in THF, DCM and DMF (Figure **S25b**). None of these three solvents has a redox window sufficiently broad that permitted the recording of the reduction of this compound, suggesting that its reduction is even more negative than that of **DABNA-1**. The E_{ox} of ***t*DABNA** is cathodically shifted compared to **DABNA-1**, having values of 0.84, 0.74, and 0.91 V vs SCE in DMF, DCM and THF, respectively; notably, as with **DABNA-1**, the E_{ox} of ***t*DABNA** is the most anodically shifted in THF. **CzBN** is only soluble in DCM (Figure **S25**c), compared to **DABNA-1** and ***t*DABNA** its E_{ox} is more positive at 1.14 V and the oxidation is reversible but **CzBN** is not as oxidizing as **4CzIPN**, **DiKTa** or **[Ir(ppy)$_2$(dtbbpy)](PF$_6$)$_2$** (E_{ox} of 1.52,[17] 1.66, [35] and 1.21 V[36] vs SCE, respectively in MeCN). The reduction of **CzBN** is likewise anodically shifted and irreversible at E_{red} of -1.69 V (Figure **S25c**) compared to those of **DABNA-1** (E_{red} = -2.24 V vs SCE in MeCN) and ***t*DABNA** (no reduction peak observed in any solvent). For comparison, **CzBN** is more reducing than **[Ir(ppy)$_2$(dtbbpy)](PF$_6$)$_2$** (E_{red} of -1.51 V vs SCE in MeCN[36]). The *tert*-butyl groups in **DtBuCzB** improved the solubility of this compound and electrochemistry could be recorded in both THF and DCM. The oxidation wave is reversible at E_{ox} of 1.21 and 1.05 V, respectively, similar in value to that of **CzBN** in DCM, while the reduction is irreversible at E_{red} of -1.77 V in DCM (the electrochemical window of THF is not sufficiently broad for the reduction to be recorded in this solvent) (Figure **S25d**). The collated electrochemical data are found in Table **1** and **S1**.

The absorption profiles of **DABNA-1**, **tDABNA**, **CzBN** and **DtBuCzB** in THF are all similar but the *tert*-butyl-substituted analogues have a more intense and red-shifted low-energy SRCT band and the SRCT band of the carbazole analogues is red-shifted compared to the DPA-based compounds due to an enhanced conjugation in the former (Figure **4c**, Table **1**). Importantly, each of these compounds has a low energy absorption band that is significantly more intense than commonly used iridium photocatalysts. For example, the ε for SRCT bands in THF of **CzBN** (λ_{abs} = 457 nm), ***t*DABNA** (λ_{abs} = 443 nm) and **DABNA-1** (λ_{abs} = 439 nm) are 48.1 × 10^3, 15.2 × 10^3 and 26.3 × 10^3 $M^{-1}cm^{-1}$, which are at least four times more intense than those of ***fac*-Ir(ppy)$_3$** (ε = 7.2 × 10^3 $M^{-1}cm^{-1}$ at λ_{abs} = 375 nm[33] in MeCN) or **[Ir(ppy)$_2$(dtbbpy)](PF$_6$)** (ε = 3.4 × 10^3 $M^{-1}cm^{-1}$ at λ_{abs} = 422 nm in THF, Figure **S54**). Notably, these bands are also more absorptive than the LRCT band of **4CzIPN** (ε = 15 × 10^3 $M^{-1}cm^{-1}$ at λ_{abs} = 369 nm in THF) (Figure **S28a**). Crucially, the molar absorptivity of the MR-TADF compounds in the blue region of the visible light spectrum is significantly higher compared to the other strongly photoreducing PCs highlighted in Figure **S3** (ε = 24 × 10^3, 14 × 10^3, 21 × 10^3 and 15 × 10^3 $M^{-1}cm^{-1}$ for **DABNA-1**, ***t*DABNA**, **CzBN** and **DtBuCzB**, respectively, in THF at 440 nm, while **Ph-PTZ** does not absorb at 440 nm).[27]

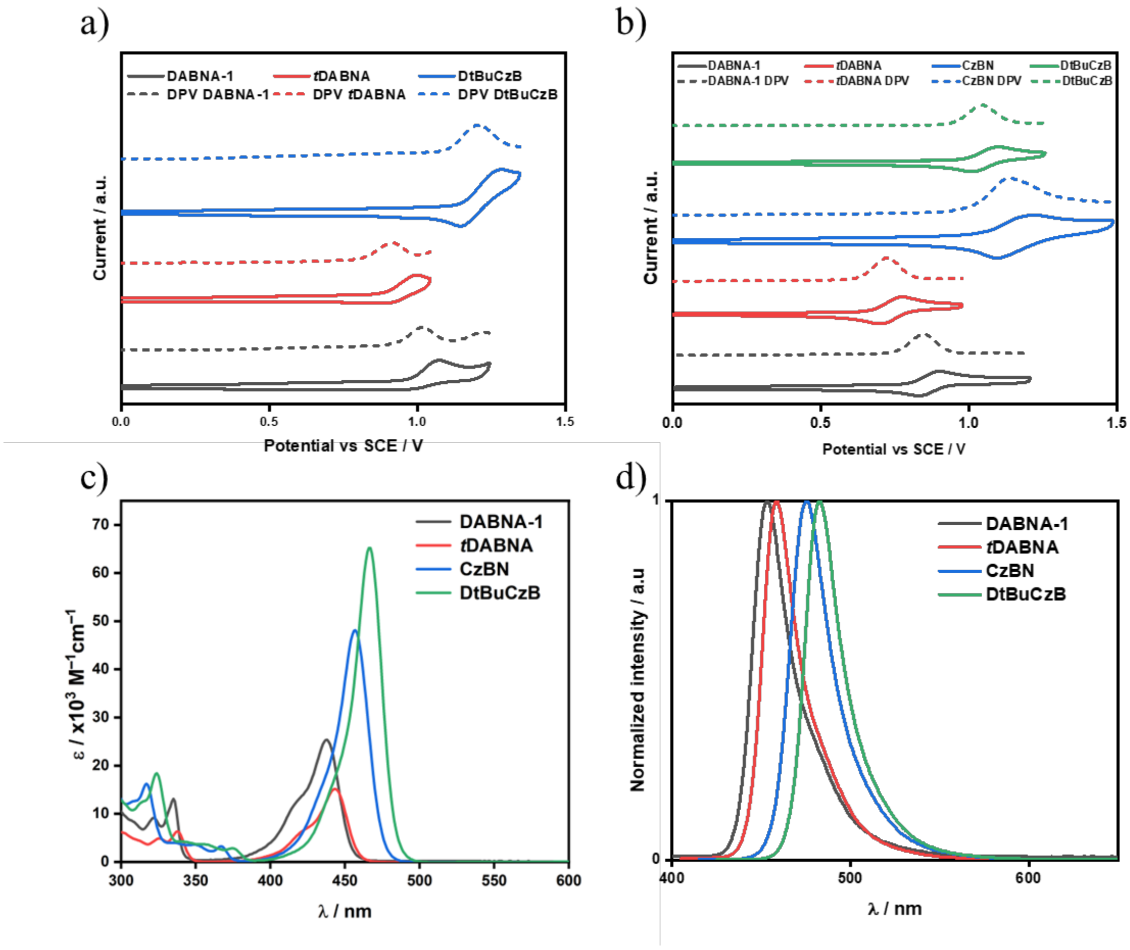

Figure 4. CVs and DPVs of **DABNA-1**, ***t*****DABNA**, **CzBN** and **DtBuCzB** in a) DCM (note **CzBN** could not be measured in this solvent), scan rate: 0.1 V/s b) THF, scan rate: 0.1 V/s. c) UV-vis absorption spectra of **DABNA-1**, ***t*****DABNA**, **CzBN** and **DtBuCzB** in THF and d) Steady-state PL spectra for **DABNA-1** (λ_{exc} = 340 nm), ***t*****DABNA** (λ_{exc} = 390 nm), **CzBN** (λ_{exc} = 400 nm) and **DtBuCzB** (λ_{exc} = 425 nm) in THF. Measurements were performed under air and at room temperature.

In THF, **DABNA-1**, **tDABNA**, **CzBN** and **DtBuCzB** emit at λ_{PL} of 453, 458, 475, 483 nm (Figure **4b**), emissions that are blue-shifted compared to that of **4CzIPN** at λ_{PL} = 528 nm (Figure **S28b**). Acquisition of the emission profiles in different solvents confirmed the small degree of positive solvatochromism (Figure **S27a**). This implies that the singlet optical gap $E_{0,0}$ for all four compounds remains broadly the same across the four solvents (Figures **S30-S34**). The largest variance in $E_{0,0}$ was observed for ***t*****DABNA** of 0.04 eV (Table **S4**). In contrast, the emission of **4CzIPN** undergoes more significant stabilization in polar media, reflected in the wider range of $E_{0,0}$ values spanning a difference of 0.10 eV. Owing in part to their large optical gaps, all four catalysts are strongly photoreducing, with E_{ox}^* = -1.91, -1.98, -1.51 and -1.55 for **DABNA-1**, ***t*****DABNA**, **CzBN** and **DtBuCzB**, respectively, in DCM. These values are much more negative than those of **4CzIPN** (E_{ox}* = -1.04 V) and **DiKTa** (E_{ox}* = -1.16 V), and comparable to those of ***fac*-Ir(ppy)$_3$** (E_{ox}* = -1.73 V in MeCN) and **Ph-PTZ** (E_{ox}* = -2.1 V in MeCN).

The singlet and triplet excited-state energies were measured in 2-MeTHF glass at 77 K (Figure **S35** and Table **S5**). The S_1 energy was inferred from the onset of the steady-state emission while the T_1 energy was determined from the time-gated emission (acquisition 1-9 ms after excitation). **DABNA-1** has the highest excited-state energies of the four compounds (S_1 = 2.81 eV, T_1 = 2.65 eV) while **DtBuCzB** has the lowest energies (S_1 = 2.66 eV, T_1 = 2.52 eV). Their excited-state energies are comparable to those of **DiKTa** (S_1 = 2.82 eV, T_1 = 2.62 eV in toluene) and ***fac*-Ir(ppy)$_3$** (T_1 = 2.50 eV in MeCN).[33]

Table **1**. Selected optoelectronic properties of **DABNA-1**, ***t*DABNA**, **CzBN** and **DtBuCzB** and the literature known photocatalysts **4CzIPN**, ***fac*-Ir(ppy)$_3$**, **DiKTa**, **Ph-PTZ**.[a]

Compound	λ_{abs} / nm	λ_{PL} / nm	$E_{0,0}$ / eV	E_{ox} / V	E_{red} / V	E_{ox}* / V	E_{red}* / V	E_{T1} / eV
DABNA-1	438	461	2.76	0.85	-2.24[b]	-1.91	0.52[b]	2.65
***t*DABNA**	444	466	2.72	0.74	/	-1.98	/	2.64
CzBN	457	480	2.65	1.14	-1.69	-1.51	0.96	2.58
DtBuCzB	467	488	2.60	1.05	-1.77	-1.55	0.83	2.52
4CzIPN	376	544	2.60	1.52[c]	-1.21[c]	-1.04[c]	1.35[c]	2.56[c]
***fac*-Ir(ppy)$_3$**[d]	375	494[e]	2.53[f]	0.77	-2.19	-1.73	0.31	2.50
[Ir(ppy)2(dtbbpy)]PF$_6$[g]	415s	591	2.17	1.21	-1.51	-0.96	0.66	2.52
[Ru(bpy)$_3$](PF$_6$)$_2$[h]	452	615	2.10	1.29	-1.33	-0.81	0.77	2.12[i]
DiKTa[j]	436	467	2.82	1.66	-1.33	-1.16	1.49	2.62[k]
Ph-PTZ[l]	< 300	445	2.78	0.68	/	-2.10	/	

[a] Values reported in dichloromethane unless otherwise noted. λ_{abs} is the lowest energy absorption band. $E_{0,0}$ is determined by the intersection between normalised absorption and emission spectra (Figure **S30-S34**). Redox potentials are given vs SCE and are obtained from the maxima in the DPV of the reduction and oxidation peaks. Excited-state redox potentials were calculated from $E_{ox}* = E_{ox} - E_{0,0}$ and $E_{red}* = E_{red} + E_{0,0}$. E_{S1} and E_{T1} were determined by the onsets of the steady-state and delayed emission spectra (measured 1 ms after excitation with gate time of 9 ms), respectively, measured in 2-MeTHF glass at 77 K. [b] Measured in MeCN. [c] Taken from Ref [17] in MeCN. [d] Taken from Refs [33,34]. [e] Measured in alcoholic glass. [f] in 2-MeTHF from Ref [37]. [g] Taken from Refs [36,38,39] in MeCN. [h] Taken from Refs [40-42] in MeCN. [i] Measured in aqueous solution. [j] Taken from Ref [35] in MeCN. [k] Measured in toluene. [l] Taken from Refs [27,32] in MeCN.

We next assess the photostability of the four compounds in each of the solvents by comparing their absorption spectra before and after photoexcitation using a 440 nm LED (Figure **S26**). The absorption spectra of all four compounds in MeCN remained broadly unchanged. In THF, the diphenylamine-based emitters **DABNA-1** and ***t*DABNA** were found to be photostable, showing no obvious changes in the absorption spectra (Figure **S36a** and **b**); however, the SRCT band in the absorption spectra of **CzBN** and **DtBuCzB** after irradiation is significantly blue-shifted (Figure **S36c** and **d**). Curiously the opposite phenomenon was observed in DCM where there is no appreciable change in the absorption spectra of **CzBN** and **DtBuCzB**, while the SRCT band in **DABNA-1** and ***t*DABNA** is red-shifted. Considering the structural differences between **DABNA-1** and ***t*DABNA** compared to **CzBN** and **DtBuCzB**, it is evident that the inclusion of diphenyl amine groups leads to an increased photostability in THF, while the structures with carbazole are more photostable in DCM.

Photocatalysis

Oxidative Quenching Photoredox Catalysis

Given the strong photoreducing power of all four PCs, we explored their use in the challenging dehalogenation reaction of aromatic halides. Methyl 4-chlorobenzoate has a reduction potential of E_{red} = -2.0 V measured in MeCN (Figure **S45**). **Ph-PTZ** has been reported to photoreduce this substrate in 100% yield in MeCN.[25] Previously reported reaction conditions include the use of an amine as a sacrificial reductant to regenerate PC from $\mathrm{PC}^{\cdot+}$ following oxidative quenching with methyl 4-chlorobenzoate. However, in order to mechanistically exclude halogen-atom transfer (XAT), where the radical cation of the sacrificial amine extracts the halogen atom from the substrate,[43] we adjusted the reaction conditions to intercept the aryl radical with 1,3,5-trimethoxybenzene (TMB).

Both **Ph-PTZ** and **DABNA-1** (Table **2**, Entries 2 and 5) can promote the quantitative dehalogenation of methyl 4-chlorobenzoate; however, coupling with the radical trap is not efficient and results in a roughly 50:50 mixture of dehalogenated product to coupled product for **Ph-PTZ** as well as **DABNA-1**. In MeCN-d_3 only the coupled product was observed in both the ^{1}H NMR spectrum and the GC-MS, implying that the proton needed for the dehalogenated product (**2**) is abstracted from the solvent (Figure **S44**). Using pivalonitrile instead of acetonitrile as the solvent led to a slight improvement in the ratio of coupled product to dehalogenated product (Table *2*, Entry 7; however, this was accompanied by an overall drop in yield.

Table **2**. Dehalogenatative cross-coupling reactions between methyl 4-chlorobenzoate (MCB) and 1,3,5-trimethoxybenzene (TMB).[a]

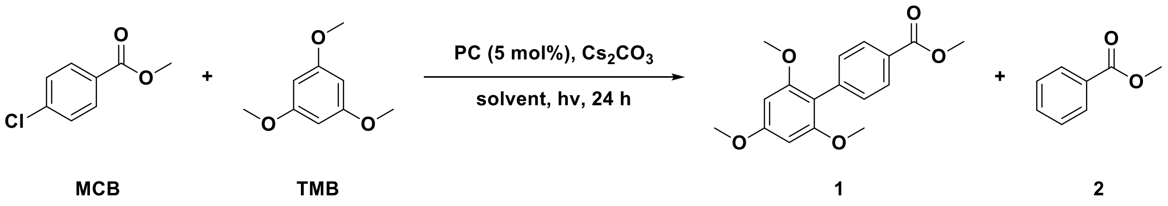

Entry	Photocatalyst	Condition	Yield 1 / %	Yield 2 / %
1	**None**	λ_{exc} = 440 nm, MeCN	0 ± 0	0 ± 0
2	**Ph-PTZ**	λ_{exc} = 390 nm, MeCN	47 ± 5	49 ± 2 (quant.[b])
3	**Ph-PTZ**	λ_{exc} = 440 nm, MeCN	Trace	Trace
4	**Ph-PTZ**	λ_{exc} = 390 nm, MeCN, 10 equiv. TMB	65 ± 1	34 ± 5
5	**DABNA-1**	λ_{exc} = 440 nm, MeCN	47 ± 4	48 ± 2
7	**DABNA-1**	λ_{exc} = 440 nm, Pivalonitrile	34 ± 1	19 ± 1
6	**4CzIPN**	λ_{exc} = 440 nm, MeCN	0 ± 0	0 ± 0
7	***fac*-Ir(ppy)$_3$**	λ_{exc} = 440 nm, MeCN	Trace	Trace
8	**[Ru(bpy)$_3$](PF$_6$)$_2$**	λ_{exc} = 440 nm, MeCN	0 ± 0	0 ± 0
9	**DABNA-1**	λ_{exc} = 440 nm, THF	0 ± 0	18 ± 1
10	***t*DABNA**	λ_{exc} = 440 nm, THF	0 ± 0	17 ± 0
11	**CzBN**	λ_{exc} = 440 nm, THF	0 ± 0	26 ± 2
12	**DtBuCzB**	λ_{exc} = 440 nm, THF	0 ± 0	21 ± 0

[a] MCB (0.1 mmol), TMB (0.5 mmol), Cs_2CO_3 (0.2 mmol), PC (5 mol%) in 1 mL solvent under a nitrogen atmosphere. Irradiated for 24 h at RT. Yield determined by ^{1}H NMR spectroscopy using 1,3-dinitrobenzene or dibromomethane as an internal standard, averaged over two experiments. [b] Literature reported yield after 24 h in MeCN using NBu_3 and HCO_2H as an additive and λ_{exc} = 380 nm.[25]

Both **Ph-PTZ** and **DABNA-1** act as equally good PCs for this reaction; however, lower energy excitation can be used with **DABNA-1** (Table **2**, Entry 5), while at 440 nm trace product is formed using **Ph-PTZ** (Table **2**, contrast Entries 2 and 3). This is important as certain organic compounds absorb at 390 nm but not at 440 nm. For example, the use of methyl 4-iodobenzoate yielded 21% of **1** and 19% of **2** in the absence of a PC when irradiated at 390 nm, but no reaction was observed when the substrate was irradiated at 440 nm (Table **S11**). When using **DABNA-1** as a PC in the reaction with methyl 4-iodobenzoate, the products **1** and **2** were formed in yields of 24 and 27%, respectively (Table **S10**). When **Ph-PTZ** is used as the PC (λ_{exc} = 390 nm), yields of 33 and 40% for **1** and **2**, respectively, were obtained, largely mirroring the efficiency of the background reaction (Table **S10**). Upon irradiation at 440 nm, none of **4CzIPN** (E_{ox}* = -1.04 V)[17], **[Ru(bpy)$_3$](PF$_6$)$_2$** (E_{ox}* = -0.81 V)[44] and ***fac*-Ir(ppy)$_3$** (E_{ox}* = -1.73 V)[34] could photocatalyzed the reaction (Table **2**, Entry 6-8), this owing to their insufficient photoreducing power to reduce methyl 4-chlorobenzoate (E_{red} = -2.0 V).

Surprisingly, Stern-Volmer quenching studies revealed that there is no quenching of the emission of **DABNA-1** with either the aryl halide or TMB. We thus investigated whether there is the formation of an electron donor-acceptor (EDA) complex by UV-visible absorption spectroscopy between the electron-rich TMB and the aryl halide for all three aryl halides. The absorption spectra revealed no emergence of a low-energy band and thus we concluded that there is no evidence of the formation of EDA complexes in these solutions. We then studied the photostability of **DABNA-1** under the reaction conditions by comparing the absorption of the reaction mixture prior to and after photoexcitation. The absorption spectrum of the reaction mixture is the same as **DABNA-1** in MeCN prior to irradiation, but it changes significantly post reaction, pointing to a photoinstability of the PC under the reaction conditions (Figure **S45c**). Thus, **DABNA-1** for this reaction acts as a pre-photocatalyst. We then studied the photodegradation of the PC and the formation of **1** and **2** as a function of time by ^{1}H NMR and absorption spectroscopy (Figure **5**). After 30 minutes, the intensity of the SRCT absorption band of **DABNA-1** decreased in intensity to 84% of its original, while the dehalogenated product was detected only in trace amounts. The intensity of this band decreased steadily to 27% of its original intensity at 5 hours, while the yield of the dehalogenated product plateaued at 35%; however, after 24 h there is complete dehalogenation of methyl 4-chlorobenzoate.

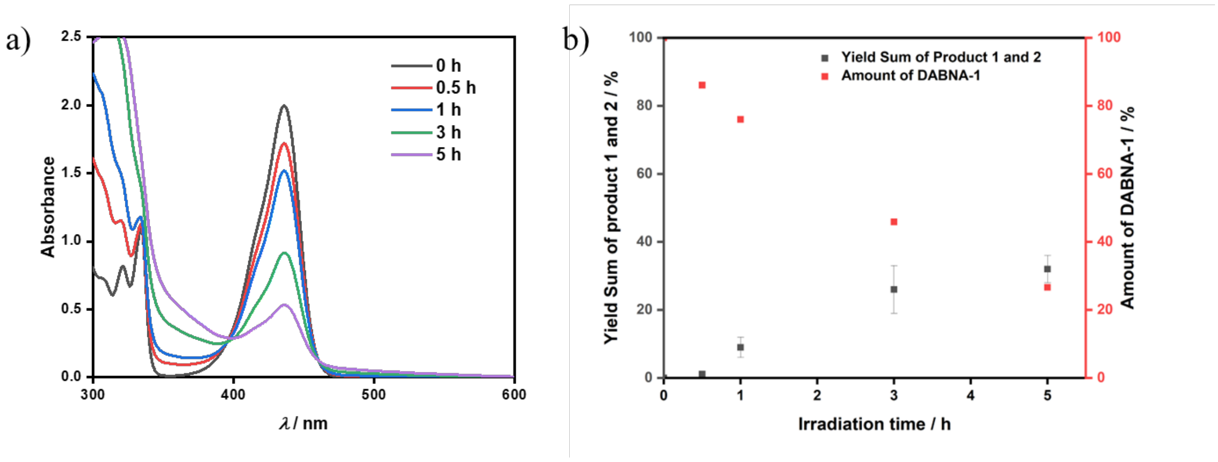

Figure **5**. Time-dependent study of the degradation of **DABNA-1** and the formation of dehalogenated product in the dehalogenation reaction outlined in Table 2. MCB (0.1 mmol), TMB (0.5 mmol), Cs_2CO_3 (0.2 mmol), PC (5 mol%) in 1 mL MeCN under inert conditions, Irradiated at 440 nm. 12 reactions were run in parallel of which three were analyzed after the given time elapsed, one for absorption measurement and two for determining the average yield and error by ^{1}H NMR spectroscopy in $CDCl_3$ using CH_2Br_2 as an internal standard. The % yield represents the combined yield of **1** and **2**. For the absorption measurements, after each time interval, 20 µL of the reaction mixture was taken and diluted further with 1 mL of MeCN before absorption measurements.

We then proceeded to assess **CzBN**, ***t*DABNA** and **DtBuCzB** as photocatalysts in the same reaction, due to their poor solubility in MeCN (and most other organic solvents), the subsequent studies were conducted in THF. Unfortunately, this solvent was problematic for this reaction as there was no evidence of **1** with these PCs nor with **DABNA-1**, while **2** was formed in yields of 18, 17, 26 and 21%, respectively, using **DABNA-1**, ***t*DABNA**, **CzBN** and **DtBuCzB**. This outcome likely is due to the more easily abstractable proton from THF than from MeCN leading to a much faster rate of a hydrogen atom transfer (HAT) from the solvent to the aryl radical than trapping with TMB. Of the four PCs, **CzBN** produced the highest yield of dehalogenated product.

We also assessed the performance of these PCs in the photocatalytic atom transfer radical addition (ATRA) reaction of styrene and *p*-toluenesulfonyl chloride (TsCl).[45,46] The generally accepted mechanism involves an oxidative quenching of the PC* by TsCl, generating a tosyl radical ($Ts^{\bullet}$), which engages in a radical addition onto the olefin. The benzylic radical is then oxidized by $PC^{+\bullet}$, regenerating the ground-state neutral catalyst and forming a cationic intermediate that is subsequently trapped by the liberated chloride anion (Figure **S46**). The reduction potential of TsCl (E_{red} = -0.94 V vs SCE)[46] is comfortably less negative than the E_{ox}^{*} of these PCs (Table **1**), meaning that all four PCs are capable of reducing TsCl. Separately, the PC$^{\bullet+}$ must be capable of oxidizing the carbon-centred radical following addition to the olefin; therefore, a moderate ground-state oxidation potential is also needed to turn over this reaction. The use of **$[Ru(bpy)_3](PF_6)_2$** (E_{ox}^{*} = -0.86 V vs SCE) as the PC has been show to yield the product in 80% in MeCN,[46] while organic D-A TADF compounds like **pDTCz-DPmS** and **4CzIPN** are not nearly as efficient, affording 16 and 10% of product, respectively, in DCM.[19] The MR-TADF library in this study was tested in this reaction as the PC in different solvents, with either one or two equivalents of styrene (

Table **3**).

Table **3**. Atom radical transfer reaction between styrene and tosyl chloride (TsCl).[a]

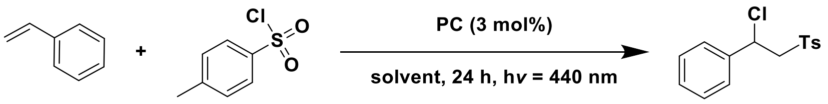

Entry	Photocatalyst	Solvent	^{1}H NMR Yield / %
1	**No catalyst**	DCM	0 ± 0
2	**DABNA-1**	THF	23 ± 1
3	**DABNA-1**	MeCN	10 ± 1
4	**DABNA-1**	DCM	56 ± 0
5	***t*DABNA**	THF	26 ± 2
6	***t*DABNA**	MeCN	7 ± 2
7	***t*DABNA**	DCM	63 ± 4
8	**CzBN**	THF	22 ± 9
9	**CzBN**	MeCN	13 ± 0
10	**CzBN**	DCM	42 ± 3
11	**DtBuCzB**	THF	17 ± 3
12	**DtBuCzB**	MeCN	11 ± 4
13	**DtBuCzB**	DCM	48 ± 5
14	**4CzIPN** (1 mol%)	DCM	39 ± 4 (10[b])
15	***fac*-$Ir(ppy)_3$** (1 mol%)	DCM	89 ± 3 (45%[c])
16	**$[Ru(bpy)_3]Cl_2$** (1 mol%)	DCM	84 ± 2 (80[c])
17	**$[Ir(ppy)_2(dtbbpy)](PF_6)$** (1 mol%)	DCM	71 ± 2

[a] TsCl (0.25 mmol), styrene (0.50 mmol) and PC (3 mol% / 1 mol%) in 1 mL solvent. Irradiated at 440 nm for 24 h at rt under a nitrogen atmosphere. Yield determined by ^{1}H NMR spectroscopy using TMB as an internal standard. [b]Literature reported yield for **4CzIPN** in DCM

after 24 h with λ_{exc} = 390 nm.[19] [c]Literature reported yield for ***fac*-Ir(ppy)$_3$** and **[Ru(bpy)$_3$]Cl$_2$** in MeCN after 24 h with λ_{exc} = 455 nm.[46]

In general, the reaction is sluggish in THF, with the highest yield of 26% being obtained using ***t*DABNA** (

Table **3**, Entry 4). A small solvent screen showed that in MeCN the yields drop drastically using each of the four PCs (

Table **3**, Entries 2, 5, 8 and 11), while switching to DCM afforded product yields of 56, 63, 42 and 48% for **DABNA-1**, ***t*DABNA**, **CzBN** and **DtBuCzB**, respectively (

Table **3**, Entries 3, 6, 9 and 12), all of which are higher than those reported using D-A TADF PCs. Product yields of 89, 84, 71, and 39%, respectively, were obtained using literature PCs **[Ru(bpy)$_3$](PF$_6$)$_2$**, ***fac*-Ir(ppy)$_3$**, **[Ir(ppy)$_2$(dtbbpy)](PF$_6$)** and **4CzIPN**. The low yield for **4CzIPN** is surprising as it should possess sufficient reducing power (E_{ox}* = -1.04 V vs SCE[17]) to reduce TsCl (E_{red} = -0.94 V vs SCE).[46]

The photostability of ***t*DABNA** was investigated under the reaction conditions (Figure **6b**). As we had shown that this compound in solution is photostable in THF but not in DCM (Figure **6a**) we wanted to determine whether there is a connection between the low yield in THF compared to DCM and the photostability of the PC. After irradiation in each of DCM and THF, the absorption profile of ***t*DABNA** changed significantly, with the complete disappearance of the low energy SRCT absorption band. This clearly shows that ***t*DABNA** is not stable under the reaction conditions regardless of the solvent used. Bryden *et al.* have shown that the of photostability of a wide range of photocatalysts engaged in photoredox reactions is generally poor.[47]

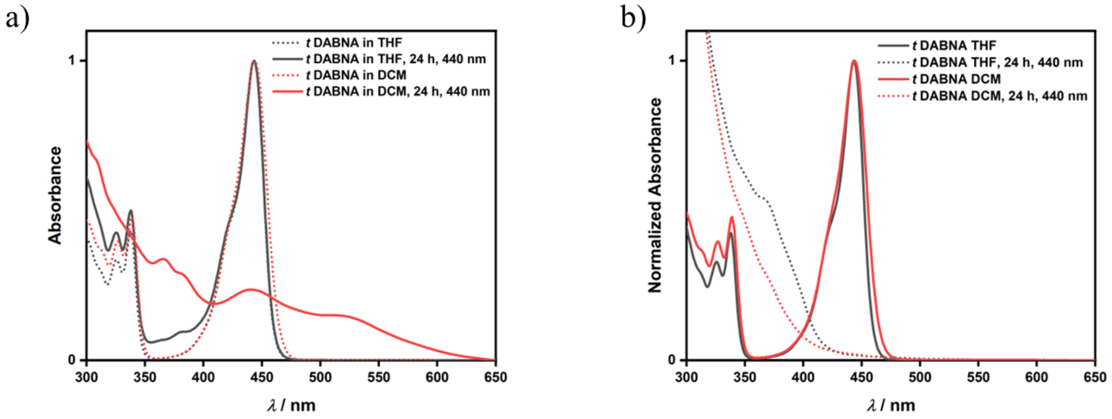

Figure **6**. Degradation study of the ATRA reaction with ***t*****DABNA** as the PC. TsCl (0.25 mmol), styrene (0.50 mmol) and PC (3 mol%) in 1 mL solvent under inert conditions. Absorption before and after 24 h irradiation at 440 nm in THF and DCM.

Reductive Quenching Photoredox Catalysis

We next selected the pinacol coupling of benzaldehyde as a model reductive quenching reaction, which involves PET from the sacrificial reductant, diisopropylethylamine (DIPEA), to the of PC* to form $PC^{-\bullet}$, which then reduces benzaldehyde with the assistance of DIPEA$^{+\bullet}$ (Figure **S50**).[48]

Table **4**. Photocatalyzed pinacol coupling of benzaldehyde.[a]

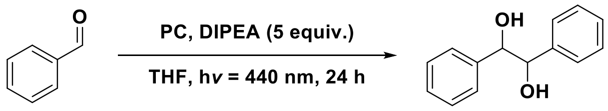

Entry	Photocatalyst	^{1}H NMR Yield / %	E_{red}* / V	E_{red} / V
1	**No PC**	0 ± 0	/	/
2	**DABNA-1** (3 mol%)	64 ± 2 (29 ± 0)	0.52	-2.24
3	***t*DABNA** (3 mol%)	61 ± 4 (35 ± 4)	n.d.[b]	n.d.[b]
4	**CzBN** (3 mol%)	70 ± 1 (0 ± 0)	0.96	-1.69
5	**CzBN** (3 mol%), 2 h	36 ± 0	0.96	-1.69
6	**CzBN** (3 mol%), dark	0 ± 0	0.96	-1.69
7	**DtBuCzB** (3 mol%)	53 ± 0 (0 ± 0)	0.83	-1.77
8	***fac*-Ir(ppy)$_3$** (1 mol%)	26 ± 2 (19 ± 1)	0.31	-2.19
9	**[Ru(bpy)$_3$](PF$_6$)$_2$** (1 mol%)	3 ± 1 (0 ± 0)	0.77	-1.33
10	**4CzIPN** (1 mol%)	71 ± 1 (73 ± 2); 68[c]	1.35	-1.21
11	**4CzIPN** (1 mol%), 2 h	50 ± 0	1.35	-1.21
12	**[Ir(ppy)$_2$(dtbbpy)](PF$_6$)** (1 mol%)	70 ± 4 (77 ± 2); 44[d]	0.66	-1.51
13	**[Ir(ppy)$_2$(dtbbpy)](PF$_6$)** (1 mol%), 2 h	69 ± 2	0.66	-1.51

[a] Benzaldehyde (0.2 mmol), DIPEA (1.0 mmol), PC (3 mol% / 1 mol%) in 1 mL solvent. Irradiated at 440 nm for 24 h at rt. Yield determined by ^{1}H NMR spectroscopy using TMB as an internal standard. Reactions carried out under an inert atmosphere and yields in parentheses are under air. [b] Reduction potential of ***t*DABNA** could not be determined in any solvent due to the too limited solvent windows. [c] Literature reported yield after 2 h in DMF and λ_{exc} = 390 nm.[19] [d] Literature reported yield after 15 h in MeCN and λ_{exc} = 450 nm, 11 W CFL.[48]

Gratifyingly, a yield of 70% was obtained using **CzBN** as the PC under a nitrogen atmosphere after 24 hours (Table **4**, Entry 4). The yields were slightly lower using **DABNA-1**, ***t*DABNA** and **DtBuCzB** at 64, 61 and 53%, respectively (Table **4**, Entries 2, 3 and 7). Decreasing the reaction time to 2 h resulted in a much lower yield of 36% (Table **4**, Entry 5). The literature accepted mechanism involves a reductive quench of the PC* by DIPEA, which means that the E_{red}* of the PCs should be more positive than the oxidation potential of DIPEA (E_{ox} = 0.86 V vs SCE)[49] for the reaction to be exergonic. With E_{red}* = 0.96 V vs SCE for **CzBN** in THF,

CzBN is the only PC of the four in the study that possesses a more positive E_{red}* than the E_{ox} of DIPEA. Control reactions under air led to no product formation using either **CzBN** or **DtBuCzB** (Table **4**, Entries 4 and 7 in parentheses); however, product yields of 29 and 35% were obtained using **DABNA-1** and ***t*DABNA**, respectively, (Table **4**, Entries 2 and 3 in parentheses). One possible reason for this divergence in behaviour would be the increased photostability of these two compounds in air under the reaction conditions compared to **CzBN** or **DtBuCzB** as demonstrated in (Figure **7a** and **b**) for two exemplar PCs, **DABNA-1** and **CzBN**. There are minimal changes in the absorption profiles of the reaction mixture with **DABNA-1** under both an inert and aerated atmosphere after irradiation compared to the profiles before absorption, suggesting that **DABNA-1** is mostly photostable in these conditions. The slight change of the absorption spectra at higher energy is more pronounced under aerated conditions, which may exmplain the lower yields in air with this PC. The time-resolved PL decays of **DABNA-1** and **CzBN** under nitrogen in THF are similar, possessing a major prompt fluorescence component with lifetimes, τ_{p}, of 10.4 and 7.6 ns, respectively, and a minor delayed fluorescence component with lifetimes, τ_{d}, of 42.3 and 58.8 μs, respectively (Figure **S53**). Under air, the delayed fluorescence is completely quenched in both compounds while the τ_{p} decrease modestly 7.0 and 6.2 ns for **DABNA-1** and **CzBN**, respectively. Thus, there seems to be no correlation between competitive quenching of the excited state of these two PCs by O_2 and reaction yield, and it is at present unclear where there is such a divergence in reactivity between these two PCs under air other than the general photoinstability of **CzBN**.

For **CzBN**, however, the absorption profiles under both inert and aerated atmospheres changed significantly after irradiation, implying that **CzBN** is unstable under these conditions. It is not evident why there is such a divergent photostability behavior between these two photocatalysts nor how this is correlated to reaction yield.

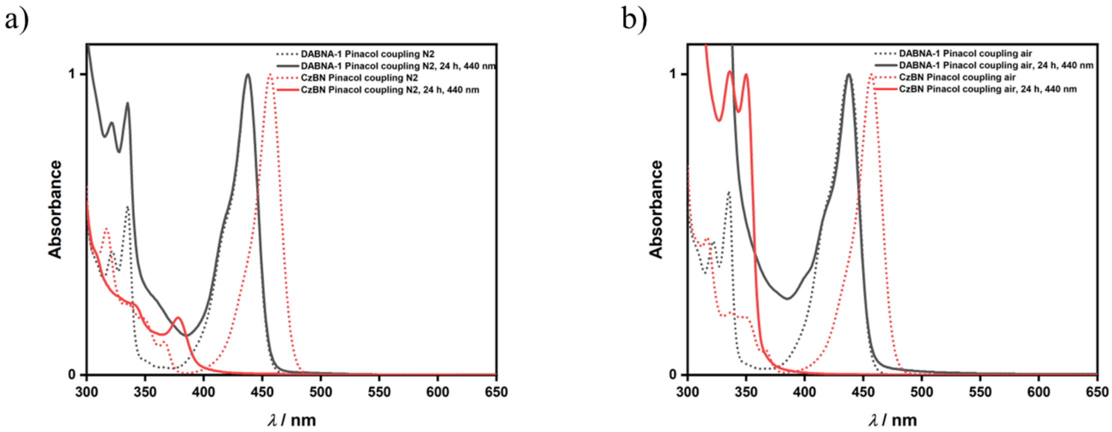

Figure **7**. Degradation study of the pinacol coupling reaction with **DABNA** and **CzBN** as the PC under a) an inert atmosphere and b) an aerated atmosphere. Benzaldehyde (0.2 mmol), DIPEA (1.0 mmol) and PC (3 mol%) in THF (0.1 M). Absorption spectra before and after 24 h irradiation at 440 nm in THF.

The yields using the reference PCs ***fac*-Ir(ppy)$_3$**, **[Ru(bpy)$_3$](PF$_6$)$_2$**, **4CzIPN** and **[Ir(ppy)$_2$(dtbbpy)](PF$_6$)** in THF under aerated conditions at 1 mol% loading, which is typically used in the literature, are 19, 0, 73 and 77%, respectively (Table **4**, Entries 8, 9, 10, and 12 in parentheses). Of these PCs [E_{red}*(***fac*-Ir(ppy)$_3$**) = 0.31 V, E_{red}*(**[Ru(bpy)$_3$](PF$_6$)$_2$**) = 0.77 V, E_{red}*(**4CzIPN**) = 1.35 V and E_{red}*(**Ir(ppy)$_2$(dtbbpy)](PF$_6$)**) = 0.66 V], **4CzIPN** has the strongest thermodynamically driving force for this reaction, which may explain the high product yield using this photocatalyst, but this argument is incongruent for **[Ir(ppy)$_2$(dtbbpy)](PF$_6$)**. Under an inert atmosphere, the yields only slightly improved to 26 and 3% using ***fac*-Ir(ppy)$_3$** and **[Ru(bpy)$_3$](PF$_6$)$_2$** while when using **4CzIPN** and **[Ir(ppy)$_2$(dtbbpy)](PF$_6$)** the yield decreased slightly to 71 and 70%, respectively (Table **4**, Entries 8, 9, 10 and 12). Of the three best-performing PCs, **CzBN**, **4CzIPN** and **[Ir(ppy)$_2$(dtbbpy)](PF$_6$)**, **CzBN** has the highest molar absorptivity (ε = 21, 6, and 2 × 10^3 M^{-1} cm^{-1} for **CzBN**, **4CzIPN** and **[Ir(ppy)$_2$(dtbbpy)]PF$_6$**, respectively) at the excitation wavelength (Figure **S54**) . Thus, the reaction should proceed the fastest with this PC, assuming that the rate-determining step is the initial reductive quenching of the PC* with DIPEA. After 2 hours, the product yields were 36, 50, and 69% using **CzBN**, **4CzIPN** and **[Ir(ppy)$_2$(dtbbpy)](PF$_6$)**, respectively (Table **4**, Entries 5, 11 and 13), implying that rate-determining step is not the initial PET to the PC*.

Energy Transfer Photocatalysis

We next assessed if these four PCs could engage in Dexter PEnT photocatalysis, using the *E*/*Z* isomerization of alkenes as a model reaction. It is generally accepted that the T_1 energy of the photocatalyst should lie intermediate those of the *E* and *Z* isomers to selectively photocatalyze the isomerization of the *E* isomer to the *Z* isomer. We assessed *E*-stilbene, di*iso*propyl fumarate and cinnamyl acetate as substrates. The E_T of *E*-stilbene and di*iso*propyl fumarate are 2.2 eV[50] and 2.7 eV[51], respectively, while the triplet energies of *Z*-stilbene and di*iso*propyl maleate are E_T of 2.5 eV[50] and 3.1 eV,[51] respectively. *E*-methyl cinnamate, structurally similar to *E*-cinnamyl acetate, has a reported triplet energy of E_T of 2.38 V.[52]

Table **5**. *E*/*Z* isomerisation of cinnamyl acetate.[a]

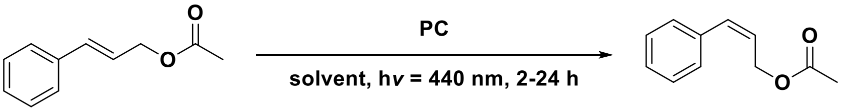

Entry	Photocatalyst	*E* / *Z* ratio	T_1[b] / eV
1	**No PC**	100/0 ± 0	/
2	**DABNA-1 (inert atmosphere), 24 h**	24/76 ± 0	2.65
3	**DABNA-1 (aerated atmosphere), 24 h**	25/75 ± 0	2.65
4	**DABNA-1 (aerated atmosphere), 2 h**	25/75 ± 0	2.65
5	***t*DABNA**	30/71 ± 1	2.64
6	**CzBN**	20/81 ± 1	2.57
7	**CzBN (dark)**	100/0 ± 0	2.57
8	**DtBuCzB**	22/78 ± 0	2.52
9	**4CzIPN**	15/85 ± 0	
10	***fac*-Ir(ppy)$_3$**	23/78 ± 4	2.50
11	**[Ru(bpy)$_3$](PF$_6$)$_2$**	100/0 ± 0	2.12

[a]Cinnamyl acetate (0.2 mmol), PC (3 mol%) in 1 mL solvent under aerated conditions unless otherwise noted. Irradiated at 440 nm for 2 h at RT. Ratio determined by ^{1}H NMR spectroscopy of an average over two experiments. [b]T_1 energy determined from the onset of the phosphorescence spectra at 77 K in 2-MeTHF glass.

DABNA-1 performed the best with cinnamyl acetate as the substrate in THF, leading to an *E*/*Z* ratio of 24/76 after 24 h under an inert atmosphere (Table *5*, Entry 2). The yield effectively did not change under aerated conditions (*E*/*Z* ratio of 25/75, Table *5*, Entry 3), implying that DET to the substrate outcompetes DET to O_2. Decreasing the reaction time to 2 hours had no effect on product yield (Table **5**, Entry 4). Using ***t*****DABNA**, **CzBN,** and **DtBuCzB** as PCs resulted in *E/Z* ratios of 30/70, 20/80, and 22/78, respectively, (Table **5**, Entries 5, 6, and 8), meaning that **CzBN** is the best PC of the four for this transformation. There seems to be a correlation between the reaction yield and the ΔE_{ST} of the PC as **CzBN** has the smallest one at ΔE_{ST} of 0.09 eV (cf. Table **1**), implying that the triplet state of **CzBN** is more readily populated as the intersystem crossing rate would be fastest for this compound. The *E/Z* ratios are comparable to those using **4CzIPN** and ***fac*****-Ir(ppy)$_3$**, while **[Ru(bpy)$_3$](PF$_6$)$_2$** could not activate the photoisomerization of cinnamyl acetate (Table **5**, Entries 5-7).

Conclusions

We have assessed the potential of four known boron-containing MR-TADF emitters as alternative photocatalysts across a mechanistically diverse range of reactions. Certain conditions resulted in our photocatalyst to not be photostable; however, this was not necessarily correlated with a reduction in product yield. Nonetheless, we found that there was variability in the photocatalyst that performed the best based on the model reactions surveyed. For instance, **DABNA-1** yielded in a complete dehalogenation of methyl 4-chlorobenzoate, ***t*****DABNA** performed the best in an ATRA reaction with a 63% yield, while **4CzIPN** yielded only 39%; further, **CzBN** is the best PC in both the pinacol coupling (70% yield; **4CzIPN** yields 71%) and the energy transfer reaction (*E*/*Z* = 20/80 for cinnamyl acetate). This study demonstrates the value of these MR-TADF compounds as PCs to enable activation of substrates with large reduction potentials while also providing versatility across a range of PET and PEnT reactions. This study reinforces the claim that MR-TADF compounds are competitive alternatives to common literature known PCs.

Acknowledgements

We would like to thank the European Union H2020 research and innovation program for the funding under the Marie S. Curie Grant Agreement (PhotoReAct, No 956324). We thank Dr. John Marques Dos Santos for supplying **DtBuCzB** and Dr Ettore Crovini for conducting initial steady-state emission studies. We thank Megan Bryden, Francis Millward and Violaine Manet for providing samples of **4CzIPN**, ***fac*****-Ir(ppy)$_3$**, **[Ir(ppy)$_2$(dtbbpy)](PF$_6$)** and **[Ru(bpy)$_3$](PF$_6$)$_2$**. We thank Prof. Daniele Leonori for discussions and for hosting L.H. for a secondment.

Supporting Information

Electronic supplementary information available: Synthetic procedures, electrochemistry, UV-vis absorption, photoluminescence spectra (room temperature steady-state, 77 K Steady-state, 77 K gated emission), photocatalysis procedure, photostability studies and Stern-Volmer quenching studies.

Table of Content

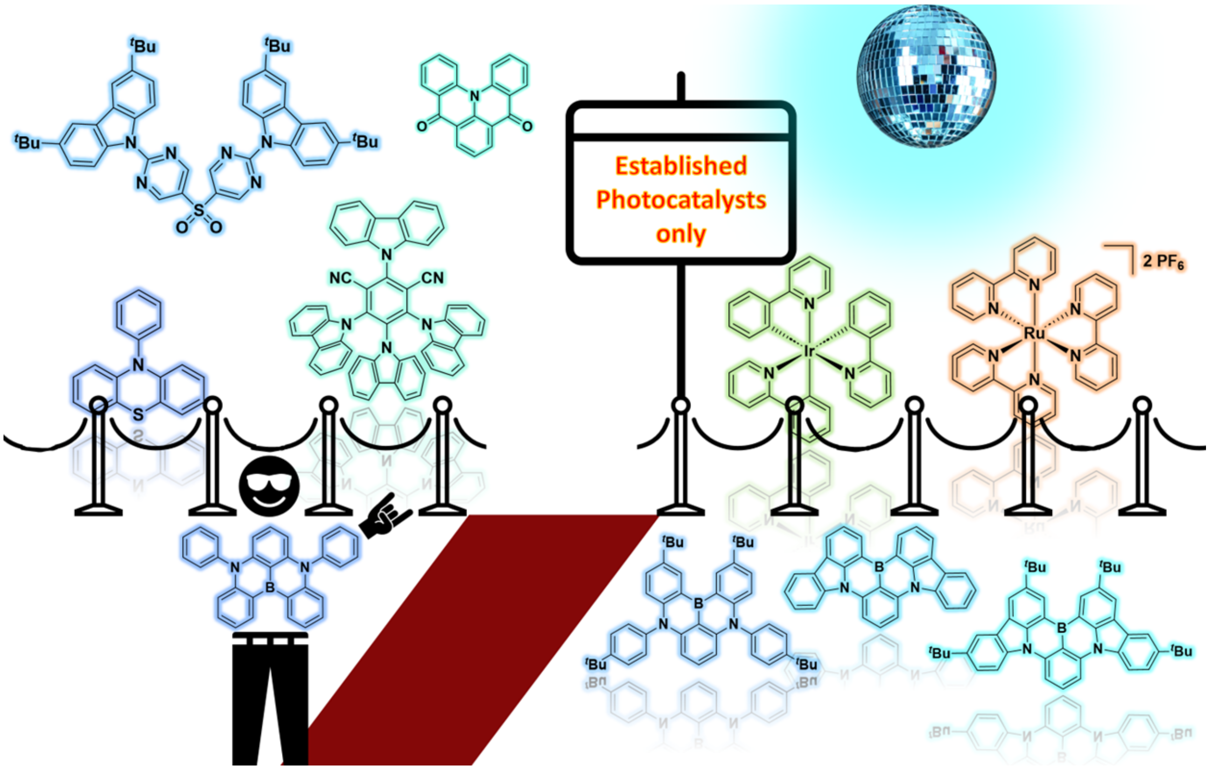

References

1. Shaw, M.H., Twilton, J., and MacMillan, D.W. (2016). Photoredox Catalysis in Organic Chemistry. J. Org. Chem. *81*, 6898-6926. 10.1021/acs.joc.6b01449.
2. Schultz, D.M., and Yoon, T.P. (2014). Solar Synthesis: Prospects in Visible Light Photocatalysis. Science *343*, 1239176. 10.1126/science.1239176.
3. Bryden, M.A., and Zysman-Colman, E. (2021). Organic thermally activated delayed fluorescence (TADF) compounds used in photocatalysis. Chem. Soc. Rev. *50*, 7587-7680. 10.1039/d1cs00198a.
4. Strieth-Kalthoff, F., James, M.J., Teders, M., Pitzer, L., and Glorius, F. (2018). Energy transfer catalysis mediated by visible light: principles, applications, directions. Chem. Soc. Rev. *47*, 7190-7202. 10.1039/c8cs00054a.
5. Ravelli, D., Fagnoni, M., and Albini, A. (2013). Photoorganocatalysis. What for? Chem. Soc. Rev. *42*, 97-113. 10.1039/C2CS35250H.
6. Romero, N.A., and Nicewicz, D.A. (2016). Organic Photoredox Catalysis. Chem. Rev. *116*, 10075-10166. 10.1021/acs.chemrev.6b00057.
7. Zeitler, K. (2018). Metal-Free Photo(redox) Catalysis. In Visible Light Photocatalysis in Organic Chemistry, C.R.J. Stephenson, T.P. Yoon, and D.W. MacMillan, eds. (Wiley-VCH), pp. 159-232.
8. Nicewicz, D.A., and Nguyen, T.M. (2014). Recent Applications of Organic Dyes as Photoredox Catalysts in Organic Synthesis. ACS Catal. *4*, 355-360. 10.1021/cs400956a.
9. Yan, D.-M., Chen, J.-R., and Xiao, W.-J. (2019). New Roles for Photoexcited Eosin Y in Photochemical Reactions. Angew. Chem. Int. Ed. *58*, 378-380. 10.1002/anie.201811102.
10. Sharma, S., and Sharma, A. (2019). Recent advances in photocatalytic manipulations of Rose Bengal in organic synthesis. Org. Biomol. Chem. *17*, 4384-4405. 10.1039/C9OB00092E.
11. Srivastava, A., Singh, P.K., Ali, A., Singh, P.P., and Srivastava, V. (2020). Recent applications of Rose Bengal catalysis in N-heterocycles: a short review. RSC Adv. *10*, 39495-39508. 10.1039/D0RA07400D.
12. Choi, W.O., Jung, Y.J., Kim, M., Kim, H., Li, J., Ko, H., Lee, H.-I., Lee, H.J., and Lee, J.K. (2023). Substituent Effects of Fluorescein on Photoredox Initiating Performance under Visible Light. ACS Omega *8*, 40277-40286. 10.1021/acsomega.3c04324.
13. Sun, W., Chen, H., Wang, K., Wang, X., Lei, M., Liu, C., and Zhong, Q. (2021). Synthesis of benzothiazoles using fluorescein as an efficient photocatalyst under visible light. Molecular Catalysis *510*, 111693. 10.1016/j.mcat.2021.111693.
14. Joshi-Pangu, A., Levesque, F., Roth, H.G., Oliver, S.F., Campeau, L.C., Nicewicz, D., and DiRocco, D.A. (2016). Acridinium-Based Photocatalysts: A Sustainable Option in Photoredox Catalysis. J. Org. Chem. *81*, 7244-7249. 10.1021/acs.joc.6b01240.
15. Tlili, A., and Lakhdar, S. (2021). Acridinium Salts and Cyanoarenes as Powerful Photocatalysts: Opportunities in Organic Synthesis. Angew. Chem. Int. Ed *60*, 19526-19549. 10.1002/anie.202102262.
16. Wong, M.Y., and Zysman-Colman, E. (2017). Purely Organic Thermally Activated Delayed Fluorescence Materials for Organic Light-Emitting Diodes. Adv. Mater. *29*, 1605444. 10.1002/adma.201605444.
17. Luo, J., and Zhang, J. (2016). Donor–Acceptor Fluorophores for Visible-Light-Promoted Organic Synthesis: Photoredox/Ni Dual Catalytic C(sp3)–C(sp2) Cross-Coupling. ACS Catal. *6*, 873-877. 10.1021/acscatal.5b02204.
18. Speckmeier, E., Fischer, T.G., and Zeitler, K. (2018). A Toolbox Approach To Construct Broadly Applicable Metal-Free Catalysts for Photoredox Chemistry: Deliberate Tuning of Redox Potentials and Importance of Halogens in Donor-Acceptor Cyanoarenes. J. Am. Chem. Soc. *140*, 15353-15365. 10.1021/jacs.8b08933.
19. Bryden, M.A., Millward, F., Matulaitis, T., Chen, D., Villa, M., Fermi, A., Cetin, S., Ceroni, P., and Zysman-Colman, E. (2023). Moving Beyond Cyanoarene Thermally Activated Delayed Fluorescence Compounds as Photocatalysts: An Assessment of the Performance of a

Pyrimidyl Sulfone Photocatalyst in Comparison to 4CzIPN. J. Org. Chem. *88*, 6364-6373. 10.1021/acs.joc.2c01137.

20. Bouzrati-Zerelli, M., Guillaume, N., Goubard, F., Bui, T.-T., Villotte, S., Dietlin, C., Morlet-Savary, F., Gigmes, D., Fouassier, J.P., Dumur, F., and Lalevée, J. (2018). A novel class of photoinitiators with a thermally activated delayed fluorescence (TADF) property. New J. Chem. *42*, 8261-8270. 10.1039/c7nj04394e.
21. Hojo, R., Bergmann, K., Elgadi, S.A., Mayder, D.M., Emmanuel, M.A., Oderinde, M.S., and Hudson, Z.M. (2023). Imidazophenothiazine-Based Thermally Activated Delayed Fluorescence Materials with Ultra-Long-Lived Excited States for Energy Transfer Photocatalysis. J. Am. Chem. Soc. *145*, 18366-18381. 10.1021/jacs.3c04132.
22. Sauvé, E.R., Mayder, D.M., Kamal, S., Oderinde, M.S., and Hudson, Z.M. (2022). An imidazoacridine-based TADF material as an effective organic photosensitizer for visible-light-promoted [2 + 2] cycloaddition. Chem. Sci. *13*, 2296-2302. 10.1039/D1SC05098B.
23. Prentice, C., Morrison, J., Smith, A.D., and Zysman-Colman, E. (2023). Multi-Resonant Thermally Activated Delayed Fluorescent (MR-TADF) Compounds as Photocatalysts**. Chem. Eur. J. *29*, e202202998. 10.1002/chem.202202998.
24. Madayanad Suresh, S., Hall, D., Beljonne, D., Olivier, Y., and Zysman-Colman, E. (2020). Multiresonant Thermally Activated Delayed Fluorescence Emitters Based on Heteroatom-Doped Nanographenes: Recent Advances and Prospects for Organic Light-Emitting Diodes. Adv. Funct. Mat, *30*, 1908677. 10.1002/adfm.201908677.
25. Poelma, S.O., Burnett, G.L., Discekici, E.H., Mattson, K.M., Treat, N.J., Luo, Y., Hudson, Z.M., Shankel, S.L., Clark, P.G., Kramer, J.W., et al. (2016). Chemoselective Radical Dehalogenation and C–C Bond Formation on Aryl Halide Substrates Using Organic Photoredox Catalysts. J. Org. Chem. *81*, 7155-7160. 10.1021/acs.joc.6b01034.
26. Theriot, J.C., Lim, C.-H., Yang, H., Ryan, M.D., Musgrave, C.B., and Miyake, G.M. (2016). Organocatalyzed atom transfer radical polymerization driven by visible light. Science *352*, 1082-1086. doi:10.1126/science.aaf3935.
27. Discekici, E.H., Treat, N.J., Poelma, S.O., Mattson, K.M., Hudson, Z.M., Luo, Y., Hawker, C.J., and Read de Alaniz, J. (2015). A highly reducing metal-free photoredox catalyst: design and application in radical dehalogenations. Chem. Commun. *51*, 11705-11708. 10.1039/c5cc04677g.
28. Hatakeyama, T., Shiren, K., Nakajima, K., Nomura, S., Nakatsuka, S., Kinoshita, K., Ni, J., Ono, Y., and Ikuta, T. (2016). Ultrapure Blue Thermally Activated Delayed Fluorescence Molecules: Efficient HOMO-LUMO Separation by the Multiple Resonance Effect. Adv. Mater. *28*, 2777-2781. 10.1002/adma.201505491.
29. Han, S.H., Jeong, J.H., Yoo, J.W., and Lee, J.Y. (2019). Ideal blue thermally activated delayed fluorescence emission assisted by a thermally activated delayed fluorescence assistant dopant through a fast reverse intersystem crossing mediated cascade energy transfer process. J. Mater. Chem. C *7*, 3082-3089. 10.1039/c8tc06575f.
30. Cai, X., Xu, Y., Pan, Y., Li, L., Pu, Y., Zhuang, X., Li, C., and Wang, Y. (2023). Solution-Processable Pure-Red Multiple Resonance-induced Thermally Activated Delayed Fluorescence Emitter for Organic Light-Emitting Diode with External Quantum Efficiency over 20 %. Angew. Chem. Int. Ed. *62*, e202216473. 10.1002/anie.202216473.
31. Xu, Y., Cheng, Z., Li, Z., Liang, B., Wang, J., Wei, J., Zhang, Z., and Wang, Y. (2020). Molecular-Structure and Device-Configuration Optimizations toward Highly Efficient Green Electroluminescence with Narrowband Emission and High Color Purity. Adv. Opt. Mater. *8*, 1902142. 10.1002/adom.201902142.
32. Treat, N.J., Sprafke, H., Kramer, J.W., Clark, P.G., Barton, B.E., Read de Alaniz, J., Fors, B.P., and Hawker, C.J. (2014). Metal-free atom transfer radical polymerization. J. Am. Chem. Soc. *136*, 16096-16101. 10.1021/ja510389m.
33. Flamigni, L., Barbieri, A., Sabatini, C., Ventura, B., and Barigelletti, F. (2007). Photochemistry and Photophysics of Coordination Compounds: Iridium. In Photochemistry and Photophysics

of Coordination Compounds II, V. Balzani, and S. Campagna, eds. (Springer Berlin Heidelberg), pp. 143-203. 10.1007/128_2007_131.

34. Koike, T., and Akita, M. (2014). Visible-light radical reaction designed by Ru- and Ir-based photoredox catalysis. Inorg. Chem. Front. *1*, 562-576. 10.1039/C4QI00053F.
35. Hall, D., Suresh, S.M., dos Santos, P.L., Duda, E., Bagnich, S., Pershin, A., Rajamalli, P., Cordes, D.B., Slawin, A.M.Z., Beljonne, D., et al. (2020). Improving Processability and Efficiency of Resonant TADF Emitters: A Design Strategy. Adv. Opt. Mater. *8*, 1901627. 10.1002/adom.201901627.
36. Lowry, M.S., Goldsmith, J.I., Slinker, J.D., Rohl, R., Pascal, R.A., Malliaras, G.G., and Bernhard, S. (2005). Single-Layer Electroluminescent Devices and Photoinduced Hydrogen Production from an Ionic Iridium(III) Complex. Chem. Mater. *17*, 5712-5719. 10.1021/cm051312+.
37. Sajoto, T., Djurovich, P.I., Tamayo, A.B., Oxgaard, J., Goddard, W.A., III, and Thompson, M.E. (2009). Temperature Dependence of Blue Phosphorescent Cyclometalated Ir(III) Complexes. J. Am. Chem. Soc. *131*, 9813-9822. 10.1021/ja903317w.
38. Chen, D.-F., Chrisman, C.H., and Miyake, G.M. (2020). Bromine Radical Catalysis by Energy Transfer Photosensitization. ACS Catal. *10*, 2609-2614. 10.1021/acscatal.0c00281.
39. Ladouceur, S., Fortin, D., and Zysman-Colman, E. (2011). Enhanced Luminescent Iridium(III) Complexes Bearing Aryltriazole Cyclometallated Ligands. Inorg. Chem. *50*, 11514-11526. 10.1021/ic2014013.
40. Juris, A., Balzani, V., Belser, P., and von Zelewsky, A. (1981). Characterization of the Excited State Properties of Some New Photosensitizers of the Ruthenium (Polypyridine) Family. Helv. Chim. Acta *64*, 2175-2182. 10.1002/hlca.19810640723.
41. Kalyanasundaram, K. (1982). Photophysics, photochemistry and solar energy conversion with tris(bipyridyl)ruthenium(II) and its analogues. Coord. Chem. Rev. *46*, 159-244. 10.1016/0010-8545(82)85003-0.
42. Juris, A., Balzani, V., Barigelletti, F., Campagna, S., Belser, P., and von Zelewsky, A. (1988). Ru(II) polypyridine complexes: photophysics, photochemistry, eletrochemistry, and chemiluminescence. Coord. Chem. Rev. *84*, 85-277. 10.1016/0010-8545(88)80032-8.
43. Constantin, T., Zanini, M., Regni, A., Sheikh, N.S., Juliá, F., and Leonori, D. (2020). Aminoalkyl radicals as halogen-atom transfer agents for activation of alkyl and aryl halides. Science *367*, 1021-1026. doi:10.1126/science.aba2419.
44. Bock, C.R., Connor, J.A., Gutierrez, A.R., Meyer, T.J., Whitten, D.G., Sullivan, B.P., and Nagle, J.K. (1979). Estimation of excited-state redox potentials by electron-transfer quenching. Application of electron-transfer theory to excited-state redox processes. J. Am. Chem. Soc. *101*, 4815-4824. 10.1021/ja00511a007.
45. Pintauer, T., and Matyjaszewski, K. (2008). Atom transfer radical addition and polymerization reactions catalyzed by ppm amounts of copper complexes. Chem. Soc. Rev. *37*, 1087-1097. 10.1039/B714578K.
46. Hossain, A., Engl, S., Lutsker, E., and Reiser, O. (2019). Visible-Light-Mediated Regioselective Chlorosulfonylation of Alkenes and Alkynes: Introducing the Cu(II) Complex [Cu(dap)Cl2] to Photochemical ATRA Reactions. ACS Catal. *9*, 1103-1109. 10.1021/acscatal.8b04188.
47. Bryden, M.A., Millward, F., Lee, O.S., Cork, L., Gather, M.C., Steffen, A., and Zysman-Colman, E. (2024). Lessons learnt in photocatalysis – the influence of solvent polarity and the photostability of the photocatalyst. Chem. Sci. *15*, 3741-3757. 10.1039/D3SC06499A.
48. Nakajima, M., Fava, E., Loescher, S., Jiang, Z., and Rueping, M. (2015). Photoredox-Catalyzed Reductive Coupling of Aldehydes, Ketones, and Imines with Visible Light. Angew. Chem. Int. Ed. *54*, 8828-8832. 10.1002/anie.201501556.
49. Goliszewska, K., Rybicka-Jasińska, K., Clark, J.A., Vullev, V.I., and Gryko, D. (2020). Photoredox Catalysis: The Reaction Mechanism Can Adjust to Electronic Properties of a Catalyst. ACS Catal. *10*, 5920-5927. 10.1021/acscatal.0c00200.
50. Herkstroeter, W.G., and McClure, D.S. (1968). Lowest triplet state of stilbene. J. Am. Chem. Soc. *90*, 4522-4527.

51. Lu, J., Pattengale, B., Liu, Q., Yang, S., Shi, W., Li, S., Huang, J., and Zhang, J. (2018). Donor-Acceptor Fluorophores for Energy-Transfer-Mediated Photocatalysis. J. Am. Chem. Soc. *140*, 13719-13725. 10.1021/jacs.8b07271.
52. Schmid, L., Kerzig, C., Prescimone, A., and Wenger, O.S. (2021). Photostable Ruthenium(II) Isocyanoborato Luminophores and Their Use in Energy Transfer and Photoredox Catalysis. JACS Au *1*, 819-832. 10.1021/jacsau.1c00137.